Desalination 325 (2013) 138–147

Contents lists available at SciVerse ScienceDirect

Desalination

journal homepage: www.elsevier.com/locate/desal

Interfacial polymerization of polyamide-aluminosilicate SWNT nanocomposite membranes for reverse osmosis ☆

Garry Nathaniel B. Baroña, Joohwan Lim, Mijin Choi, Bumsuk Jung *

Laboratory of Environmental & Energy Materials, Department of Environmental Engineering & Energy, Myongji University, Yongin, Gyeonggi-do 449-728, Republic of Korea

HIGHLIGHTS

- Single pass flow method to infuse aluminosilicate SWNT to polyamide is developed.
- SWNT incorporation increased the pure water permeance of the TFN membranes.
- High permeate flux is due to preferential water flow through hydrophilic nanotubes.
- Enhanced RO performance is ascribed to Donnan potential and steric effects.

ARTICLE INFO

Article history:
Received 1 April 2013
Received in revised form 28 June 2013
Accepted 30 June 2013
Available online 3 August 2013

Keywords:
Polyamide
Thin film nanocomposite membrane
Interfacial polymerization
Aluminosilicate single-walled nanotube
High permeate flux low pressure RO membrane

ABSTRACT

A new method of single-pass flow which incorporates aluminosilicate single-walled nanotubes (SWNT) in a polyamide matrix was developed to fabricate thin film nanocomposite (TFN) membranes for low pressure reverse osmosis (RO) via interfacial polymerization. The TFN membranes were characterized using attenuated total reflectance–Fourier transform infrared (ATR–FTIR) and X-ray photoelectron spectroscopy (XPS) for the analysis of functional groups as well as composition of SWNTs. The typical morphology of polyamide layers was observed using atomic force microscopy (AFM) and scanning electron microscopy (SEM). The introduction of SWNTs in polyamide active layer is evident with the proliferation of aluminum and silicon elements from XPS analysis. All membranes show the rugose structure with "leaf-like" outgrowths and the "ridge-and-valley" structure commonly observed in polyamide RO membranes. The hydrophilicity was increased as observed in the enhancement in water flux and pure water permeance, due to the presence of hydrophilic nanotubes. With the incorporation of the single-walled aluminosilicate nanotubes, higher permeate flux was achieved while sustaining high rejection of monovalent and divalent ions, typical of polyamide RO membrane.

1. Introduction

Reverse osmosis (RO) is the most widely used desalination technology as response to fresh water shortage and enormous global demand of drinking water. Over the last few decades, remarkable advances in the preparation of RO membranes from different materials and fabrication processes have been made. Polyamide (PA) reverse osmosis membrane is one of the most widely used membrane materials. These PA RO membranes are fabricated via interfacial polymerization (IP) of two monomers reacting in a two phase system, where polymerization takes place in the interface between the aqueous and organic phases [1]. The well-known two monomer solutions, *m*-phenylenediamine (MPD) in water phase and trimesoyl chloride (TMC) in hexane phase, have been commercially utilized to form a thin film composite (TFC) membrane. This thin film polymer film is mounted on a porous support layer through in situ polycondensation process [2]. Syntheses of PA TFC with different chemistries [3,4], surface functionalization [5,6], and post treatments [7,8], have been performed to fabricate RO membranes. However, substantial innovations in RO membrane engineering are still in high exigency because of the increasing needs for desalination membranes with enhanced permeate flux, higher salt rejection, and greater resistance to fouling [9].

The advancement in nanotechnology has enabled the introduction of the use of mixed-matrix membranes, where nanofillers are dispersed throughout a polymeric matrix. These types of membranes have generated additional degrees of freedom to the development of innovative membrane materials for numerous separation processes such as fuel cell applications, gas separation, pervaporation, and water filtration [10–13]. Currently, thin film nanocomposite (TFN), a new type of nanotechnology enhanced membrane material, is studied as prospective candidate for desalination purposes. A new fabrication strategy to manufacture TFN membrane via dispersion of inorganic fillers in the thin polymeric layers has been performed during interfacial polymerization. Several studies have shown methods on how to incorporate zeolites [14,15], silica [16], and silver [17] nanoparticles,

* Corresponding author. Tel.: +82 31 322 6694; fax: +82 31 336 6336.
E-mail address: bjung@mju.ac.kr (B. Jung).

0011-9164/$ – see front matter
http://dx.doi.org/10.1016/j.desal.2013.06.026

as well as carbon nanotubes [18], into the polyamide matrix of the TFNs. Considering the thickness of thin film layer synthesized via IP, the choice of filler is very important because surface characteristics such as hydrophilicity, zeta potential and roughness can make considerable effect on the membrane performance and durability [18]. Moreover, compatibility with matrix and size of fillers are also essential. If the size of filler is bigger than the thickness of the thin film layer, the filler would be a source of defect, which can decrease the selectivity of TFN membrane. With less even distribution of the fillers within the matrix and less compatibility with the surface of fillers, high membrane performance and good mechanical property would not be expected [19].

Recently, single-walled carbon nanotubes (SWCNTs) have been of great interest as filler materials for desalination membranes because water transport obtained through SWCNT has very high fluid fluxes. This enhanced water flux is mainly due to the atomic-scale smoothness of the nanotube walls that enable "frictionless" flow of fluids and molecular ordering phenomena observed inside the nanopore [20,21]. Although the unique properties of SWCNT offer higher diffusional flux of water in the nanopore, the hydrophobic nature of inner wall, as well as the compatibility of outer surface with PA, hinders its practical application to reverse osmosis and nanofiltration.

In this study, the incorporation of hydrophilic nanotubes within the polyamide selective layer is introduced. Fig. 1 shows the nanotube's inner diameter (d_i) of ca. 1.0 nm, and external diameter (d_o) of ca. 2.3–2.7 nm. These single-walled nanotubes have average length of approximately 100 nm [22]. Imogolite, as commonly called, has an empirical formula of $(OH)_3Al_2O_3SiOH$ and is composed of an outer wall layer of aluminum hydroxide and isolated silicate groups pendent from the inner wall [23]. The presence of hydroxyl groups, namely, (Si–OH) inner wall and Al–OH outer surface, makes the nanotube hydrophilic. As mentioned by Ohashi et al., imogolite is so hydrophilic that 1 g of the hydrophilic imogolite can absorb about 0.8 g of water at relative humidity of 90–95% [24]. In contrast with SWCNT, Beloizyky et al. reported that the diffusion of water through imogolite is 0.5×10^{-5} cm^2/s measured by NMR relaxometry, which is about four times slower than free water [25]. Using molecular dynamic simulation, Creton et al. argued that the diffusion of water through the imogolite nanotube is much slower than water vapor due to the internal surface interaction with water and the geometry of curvature [26].

A few methods to incorporate imogolite in polymer matrix, as inorganic hybrid composite materials, has been performed by blending/mixing the imogolite and matrix polymers [27,28] for new composite films and membranes [29]. However, techniques on incorporating synthetic imogolite in TFN for RO applications have not been reported. Thus, it would be interesting to investigate how membrane performance, such as water flux and rejection, would be varied as the hygroscopic nanotubes filled with water molecules, as well as freely carrying channels, compete with diffusion through PA matrix.

In the present paper, we demonstrate a new approach of interfacial polymerization of TFN PA membranes for low pressure RO, prepared with appropriate concentration of hydrophilic single-walled aluminosilicate nanotubes. Assessment of membrane performance, such as water flux and salt rejection, and structural characterization of TFC and TFN membranes will be followed by discussions on the effect of the incorporated imogolites in TFN membranes.

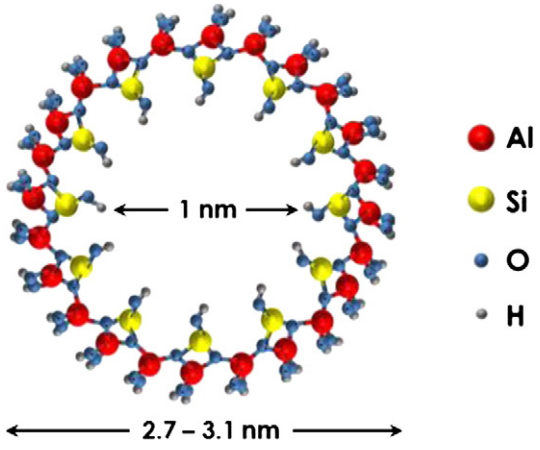

Fig. 1. Schematic illustration of the aluminosilicate single-walled nanotube.

2. Experimental

2.1. Synthesis of aluminosilicate single-walled nanotubes

The synthesis of aluminosilicate single-walled nanotubes was performed using the procedure of Farmer et al. [22,23] with modifications, as follows. Aluminum nitrate nonahydrate (Duksan Pure Chemical Co., Ltd., Korea) and tetrasodium monosilicate n-hydrate (Wako Pure Chemical Industries, Ltd., Korea) were used as the aluminum and silicon sources. The solutions were mixed and stirred for 1 h using a peristaltic pump at room temperature to make a final Si/Al ratio of 0.58. After complete dissolution, the pH of the solution was adjusted to 5.0 using 0.1 M sodium hydroxide. The solution was then adjusted to pH 4.3 by adding 0.1 M hydrochloric acid and 0.2 M acetic acid. Differing from Farmer's procedure, polyvinyl alcohol (M_w = 89 K, Sigma-Aldrich, Korea) was added, making up 0.03 wt.% of the aqueous solution. Then, the solution was left to stand for 2 h before heat treatment at 95 °C for 3 days. It was allowed to cool down to room temperature. The pH was adjusted to 8.0 using 0.1 N ammonium hydroxide to form a gel from solution. The gel was then adjusted to pH 4.0 by adding 0.1 M hydrochloric acid to redisperse the nanotubes. The resulting gel was dialyzed against deionized water for 3 days to achieve equilibrium [30]. The dialyzed imogolite solution was immersed in ethanol and in hexane for 3 days each to promote solvent exchange.

2.2. Characterization of aluminosilicate single-walled nanotubes

High resolution–transmission electron microscope (HR–TEM) observations were carried out on a JEOL JEM-3010 microscope operated at 300 kV. The camera length was calibrated with Au standard. A drop of the 0.01 mg/ml of synthesized imogolite solution was deposited on a TEM copper grid. Nitrogen adsorption measurements were also performed at 77 K using BEL-SORP max (BEL Co., Ltd., Japan) gas adsorption analyzer. The samples were first degassed for 24 h at 383 K to obtain a residual pressure in the range of 10^{-3} to 100 mm Hg. The amounts of N_2 adsorbed at relative pressures were used to investigate the total pore volumes, which corresponded to the sum of the micropore volumes. The pore size distribution of the sample was calculated using Horvath–Kawazoe method.

2.3. Preparation of thin film composite/nanocomposite membranes

TFC and TFN membranes were fabricated via interfacial polymerization using commercial polysulfone ultrafiltration (UF) membranes (Woongjin Chemical Co., Ltd., Korea) as support. The procedure was carried out using the previous methods [2,4], but with few modifications. For the TFC membrane, the rectangular cut UF membrane was first soaked in a 400-ml aqueous solution of 2% (w/v) *m*-phenylenediamine (MPD, >99%, Sigma-Aldrich, Korea) for 2 min at 25 °C. The membrane was then removed from the MPD solution and was clamped to a rectangular glass. The glass was inclined so that the excess water will drop down. A rubber roller was used to finally remove all the excess solution on the MPD-soaked support membrane. Then, 100 ml of 0.1% (w/v) of 1,3,5-benzenetricarbonyl trichloride (TMC, >98%, Tokyo Chemical Industry Co., Ltd., Japan) in hexane solution was then reacted with the top

surface of the MPD-soaked membrane for 1 min at 25 °C. After the interfacial polymerization, the TMC solution was drained off and the membrane was dried under ambient condition for 1 min. This was followed by immersion to 0.2% $NaHCO_3$ solution for 10 min. It was finally stored in deionized water prior to membrane performance [2,14,31].

The same procedure was performed for the fabrication of TFN membranes but with some additional steps. Following the removal of MPD solution from the polysulfone membrane with rubber rolling, a single pass flow of different imogolite concentrations in 0.01% (w/v) TMC-hexane solution was reacted with the top surface of the MPD-soaked membrane. It should be noted that the imogolite solution in hexane medium was agitated with ultrasonicator for 30 min to promote dispersion of imogolites before use. The imogolite solutions were mixed with 0.01% (w/v) TMC organic solution to make 0.05, 0.1, and 0.2% (w/v) imogolite concentrations. During the vigorous agitation, the agglomeration of imogolite, which could be caused by the reaction between hydroxyl groups on imogolite and acyl chloride in TMC, was not observed. After unforced evaporation of the hexane at room temperature, two rectangular silicon frames with holes were clamped together with the membrane in the middle. This created a volume where 0.1% (w/v) TMC-hexane solution, same as prepared in TFC, was poured. Membranes with 0.05, 0.1, and 0.2% (w/v) of SWNT are named as TFN-1, TFN-2 and TFN-3, respectively, in the following discussion. Fig. 2 shows the schematic diagram of the interfacial polymerization of polyamide nanocomposite membranes.

2.4. Characterization of thin film composite/nanocomposite membranes

Attenuated total reflectance-Fourier transform infrared spectroscopy (ATR-FTIR) was used to characterize the structure of the thin film composite membranes. These experiments were performed using a Bruker IFS-66/S FTIR with an ATR accessory. Spectra were collected in the mid-infrared region (400–4000 cm^{-1}), using 32 scans. The spectra of composite membranes include the polyamide layer, with and without aluminosilicate nanotubes, as well as the polysulfone support layer.

To examine the elements present on the TFC and TFN surfaces, X-ray photoelectron spectroscopy (XPS) was performed using a Thermo Scientific K-Alpha spectrometer with a monochromatic Al Kα X-ray source and high resolution per step of 0.1 eV. The spectra were taken at a sampling depth of 10 nm by a concentric hemispherical energy electron analyzer. Membranes were mounted on a sample holder without adhesive tape and kept overnight at high vacuum in the preparation chamber before they were transferred to the analysis chamber of the spectrometer for their analysis. Each spectral region was scanned for several sweeps until a good signal-to-noise ratio was observed.

Surface morphology of the samples was analyzed using scanning electron microscope (SEM) (S-3500N, Hitachi) with an accelerating voltage of 15.0 kV. The top surface and cross-section of the TFC and TFN were analyzed.

In order to quantify the concentration of imogolite in polyamide layer, it was necessary to isolate the thin films from the composite membrane layers. First, the polyester backing was carefully peeled off, and then the polyamide and polysulfone layers were immersed in chloroform. Due to selective dissolution of polysulfone to chloroform, a hazy thin film of polyamide floated on the surface of chloroform solution. Using a clean glass plate, the polyamide film was lifted up and washed several times with chloroform. After drying the collected polyamide films, appropriate amount of samples (about 10 mg) were used for thermogravimetric analysis (TGA 2950, Mettler–Toledo).

Quantitative surface roughness analysis of the composite membranes was measured using atomic force microscope (AFM) (Park Systems XEI-100E, Korea) imaging and analysis. The surface roughness of the membranes was described in terms of the root mean square roughness (R_q), root average arithmetic roughness (R_a) and the root peak-to-valley distance (R_{pv}). AFM images were acquired under ambient conditions in intermittent contact mode at 1 Hz scan rate and 256 × 256 pixel resolution with silicon cantilevers (spring constant ~ 50 N/m). The tapping mode (i.e., intermittent contact mode) was used to prevent damage to the membrane surface. Two different positions were analyzed for each membrane for a 5 μm × 5 μm sampling area.

2.5. Membrane performance evaluation

The performance measurement of the TFC and TFN membranes were tested using a laboratory-scale crossflow apparatus at a working temperature of 25 ± 2 °C. The crossflow system consists of two stainless steel test cells connected to a feed tank, a positive displacement pump and pulsation dampener (Hydra-Cell, Wanner Engineering Inc.), a back pressure regulator and bypass valve to independently control pressure (1–16 bar), and a pressure gauge. The feed solutions are continuously passed through a system of valves connected with chemical resistant stainless steel tubing. The dimensions of the test cells are 150 mm × 150 mm × 50 mm (l × w × h), with an active membrane surface area of 8.25 × 10^{-3} m^2.

The feed encounters a 90° bend as it enters the test channel. Six equally spaced bolts around the periphery of the cell secure the cell lid to the base. The permeate stream from each membrane was collected in a beaker on top of a balance. The balance is connected to a data acquisition program for continuous monitoring of water flux.

The membrane performance was measured using a detailed protocol. First, pre-compaction of the membranes was carried out at 16 bar for 30 min using deionized water. The purpose of this stage was to attain a stable membrane and permeate flux, and improve reproducibility of the results. The water flux was then measured at varying pressures

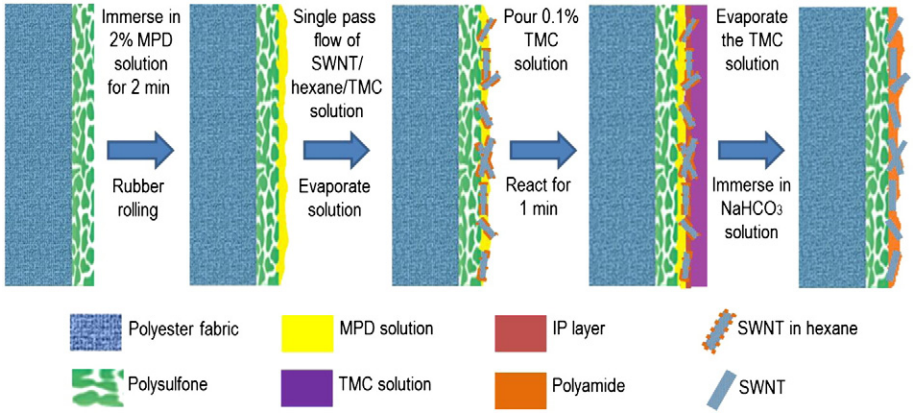

Fig. 2. Schematic diagram of the interfacial polymerization of the thin film nanocomposite membranes. The same procedure is performed to fabricate thin film composite membrane without the aluminosilicate SWNT.

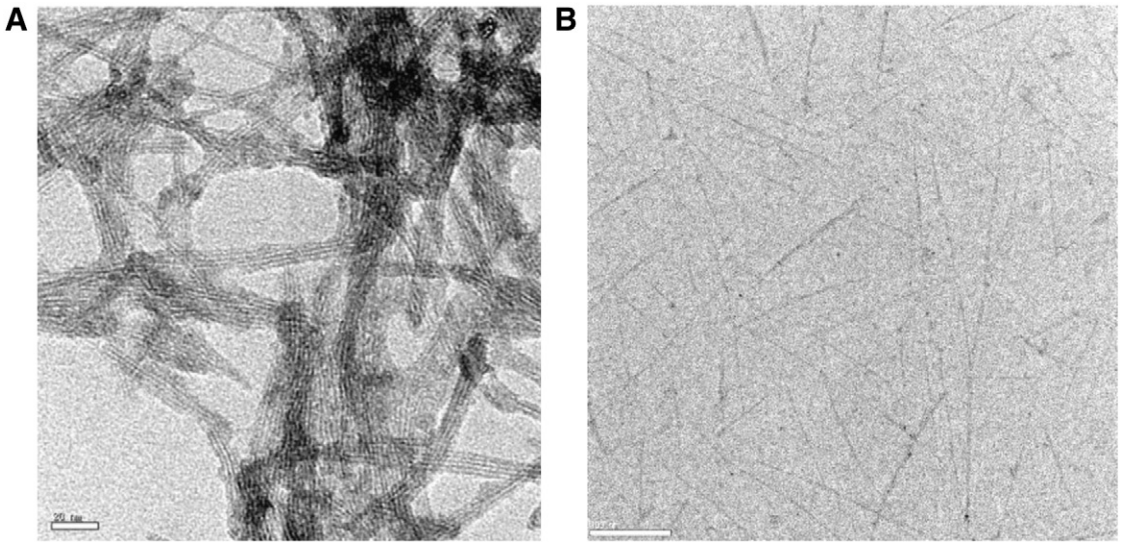

Fig. 3. TEM pictures of synthesized aluminosilicate single-walled nanotubes. (A) Agglomerated and entangled in bundles with 20 nm scale bar; (B) single well dispersed structure with 100 nm scale bar.

from 2 to 16 bar with a 2 bar increment, for 30 min each. The water flux was checked every 5 min by collecting the permeate in a beaker. After this, the deionized water was drained out from the crossflow system. The salt solution was then introduced into the system for the rejection experiments. The salt solution flux was measured at 8, 10, 12, 14, and 16 bar for 30 min each. The flux was checked every 5 min. In a vial, 10 ml of the permeate and retentate were collected every 30 min for 3 h. All reported flux and rejection data represent the averages of five separate tests of the hand-cast membranes.

The permeation flux (F) and salt rejection (R) of the membranes were calculated using Eqs. (1) and (2) [32]:

$$F = \frac{V}{At} \tag{1}$$

$$R = \left[1 - \frac{C_p}{C_f}\right] \times 100\% \tag{2}$$

where V is the volume of permeate solution during the test time, A is the effective membrane area, and t is the test time, respectively, and C_p and C_f are the salt concentration of permeate solution and feed solution, respectively.

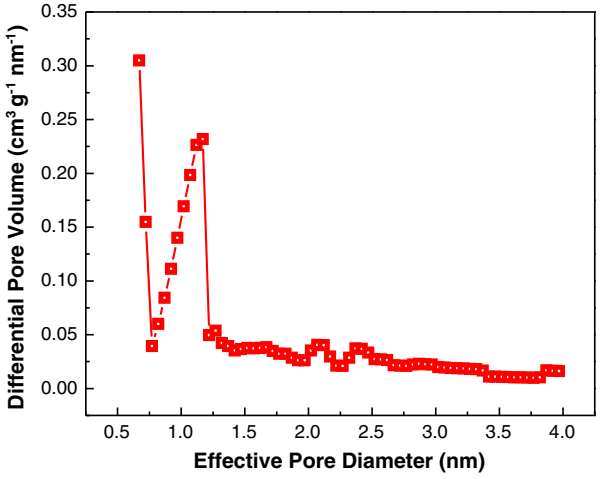

Fig. 4. Differential pore size distribution of the aluminosilicate single-walled nanotubes obtained from nitrogen adsorption data using Horvath–Kawazoe method.

In all experiments, the NaCl and Na_2SO_4 concentrations were determined by measuring the permeate and retentate conductivities using a conductivity meter (Orion 3-Star Plus Conductivity Benchtop Meter). A calibration curve allowed the determination of salt concentration from measured solution conductivity.

3. Results and discussion

3.1. Characterization of aluminosilicate single-walled nanotube

3.1.1. High resolution–transmission electron microscopy (HR–TEM)

As can be seen in Fig. 3(a), HR–TEM of the synthesized imogolite shows a spiderweb-like network structure where occasionally individual tubes may be distinguished. It consists mainly of fibers, which are entangled and aligned in bundles when water was used for dispersion medium. This bundling effect was also observed in electron micrographs of natural imogolite [33] and other synthetic imogolite owing to the surface charge [22,30]. In Fig. 3(b), the aluminosilicate single-walled nanotubes were well observed when dispersion of SWNT with hexane was used. The average length of SWNT is about 150 nm long and the average outer diameter of these fibers is roughly 2.7 nm, which is comparable to previously prepared synthetic imogolites [34,35].

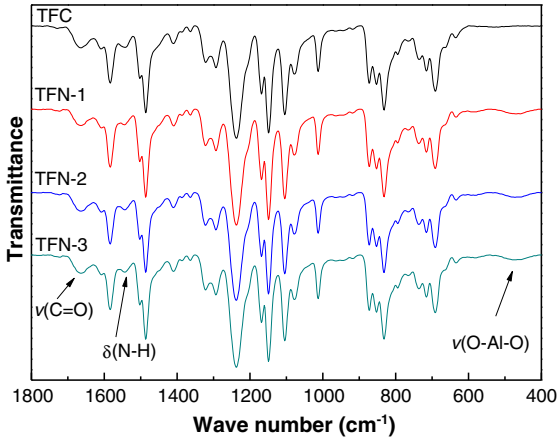

Fig. 5. ATR-FTIR spectra of TFC and TFN membranes.

Table 1
Elemental atomic concentrations of the TFC and TFN membranes.

Name	Con. of IG (vol.%)	Loaded amount of IG (wt.%)	C (%)	N (%)	O (%)	Al (%)	Si (%)	Si/Al	C/N	CL[a] (%)
TFC	0	0	73.38	11.98	14.63	0.00	0.00	0.00	6.13	91.65
TFN-1	0.05	0.15	71.54	11.19	15.13	1.38	0.76	0.55	6.39	73.79
TFN-2	0.1	0.23	71.23	10.97	15.38	1.58	0.84	0.53	6.49	67.12
TFN-3	0.2	0.59	71.08	10.86	15.46	1.70	0.90	0.53	6.55	63.66

[a] CL = degree of cross-linking.

3.1.2. Nitrogen adsorption

In order to ascertain the effective pore diameter of the aluminosilicate single-walled nanotubes, nitrogen adsorption was performed. Using the Horvath–Kawazoe method [36], the differential pore size distribution curve was determined. Fig. 4 shows that the synthesized nanotubes demonstrate one maximum within the distribution regime, indicating a monodisperse hollowed structure of the aluminosilicate SWNTs. The monomodal distribution is centered at effective pore diameter of 1.17 nm. The results are in good agreement with earlier studies on natural and synthesized imogolites [37,38].

3.2. Characterization of thin film nanocomposite membrane

3.2.1. ATR–FTIR and XPS analyses

In order to show the successful interfacial polymerization of polyamide and incorporation of the aluminosilicate nanotubes, ATR–FTIR and XPS analyses were performed. Fig. 5 shows the ATR–FTIR spectra of the TFC and TFN membranes. From the IR spectra, the membranes showed identical peaks with that of a polyamide which indicates that interfacial polymerization has occurred to all of the membranes [39]. A strong band at 1660 cm^{-1} which represents the amide I band, a characteristic of C═O bands of an amide group, is present. In addition to this, other bands are also seen at 1542 cm^{-1} (amide II band for the N – H in-plane bending), 1610 cm^{-1} (C═C ring stretching vibration), and 1720 cm^{-1} (C═O stretching of carboxylic acid) [4,39]. For the TFN membranes, transmittance band at a low frequency of 469 cm^{-1}, which is associated with O – Al – O and Al – OH groups, are observed.

In order to quantify the amount of SWNTs within polyamide layers mentioned in Section 2.4, thermo-gravimetric analysis (TGA) was performed. The amount of aluminosilicate nanotubes in the polyamide nanocomposites were characterized by measuring the residue after thermal decomposition of polyamide/polyamide nanocomposites under air atmosphere. The concentration of imogolite in TMC organic solutions and the actual loaded amount of aluminosilicate single-walled nanotubes in the PA layer are listed in Table 1.

To further elucidate the presence of aluminosilicate SWNTs within the polyamide matrix, the chemical composition of the polyamide active layer was determined using the X-ray photoelectron spectroscope. Since the RO membrane is a composite membrane consisting of polyamide on a polysulfone support, the XPS depth profile was fixed to 10 nm in order to probe the near surface region of the polyamide film only and not the polysulfone. The elements studied were C, N, and O, which are elemental characteristics of the polyamide. In order to investigate the incorporation of aluminosilicate nanotubes, elemental Al and Si of the TFN membranes were also probed. The C(1)s, N(1)s, O(1)s, Al(2)p and Si(2)p spectra of the membranes are illustrated in Fig. 6. Table 1 presents the atomic concentration percentages, Si/Al and C/N ratios, and the degree of cross-linking of the TFC and TFN membranes.

It can be observed that the TFN membranes contain Al and Si elements. The elemental percentages of Al and Si increase as the imogolite concentrations increase. The presence of these elements in the XPS analysis shows that the aluminosilicate nanotubes were successfully embedded in the polyamide matrix. The Si/Al ratios of

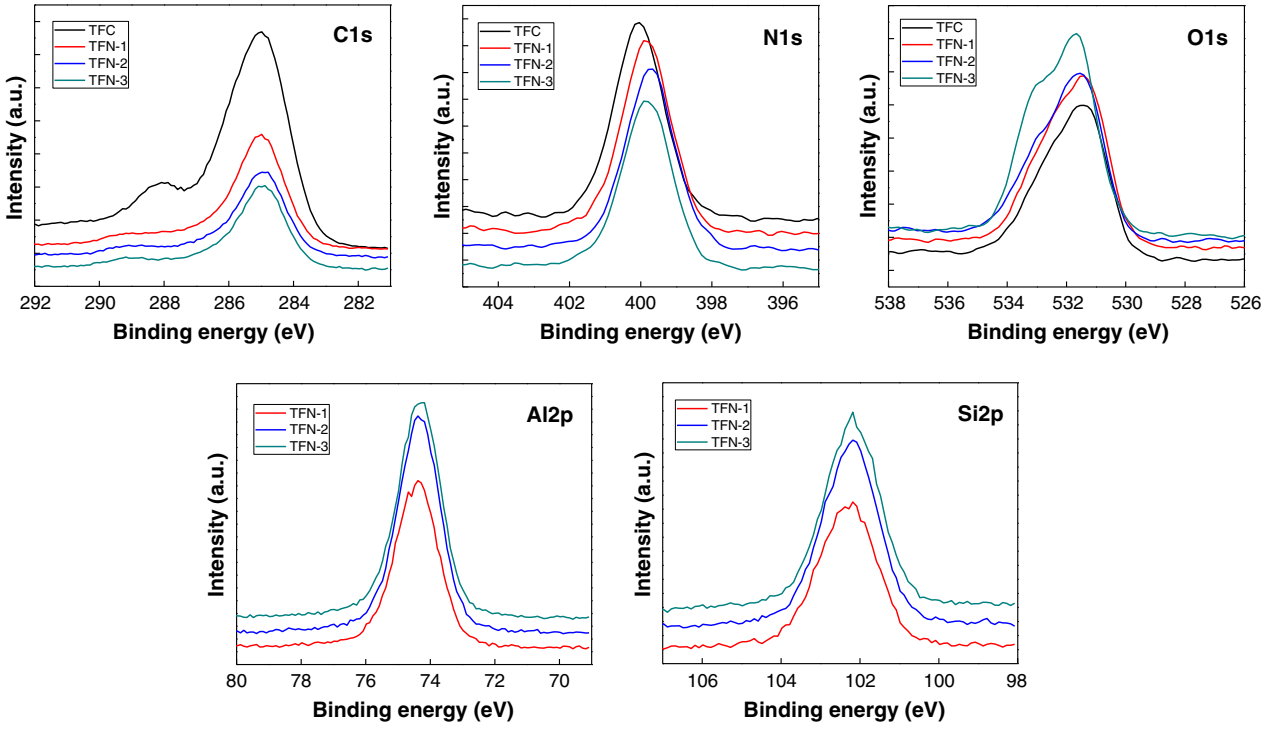

Fig. 6. C(1)s, N(1)s, O(1)s, Al(2)p, and Si(2)p spectra of the TFC and TFN membranes.

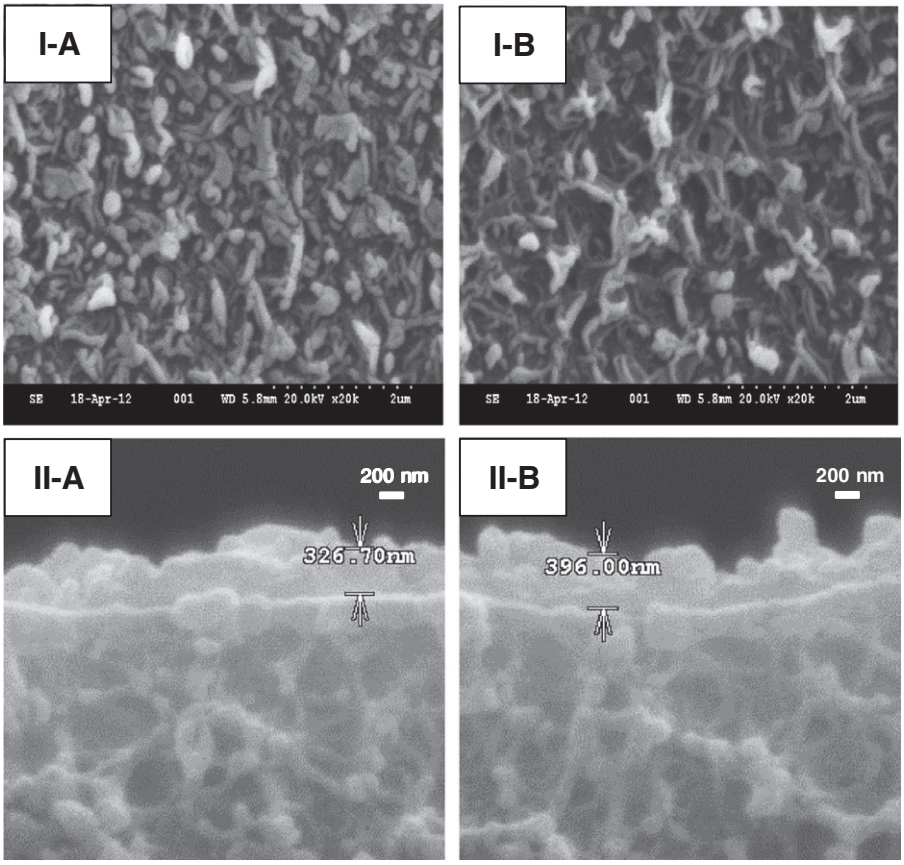

Fig. 7. SEM images of polyamide TFC (A) and TFN-3 (B) membranes. Top surface (I) and cross section (II) images are presented.

the TFN membranes also show comparable results to the Si/Al ratio of 0.58 during the synthesis of the nanotubes, as described in Section 2.1.

Since the polyamide backbone has cross-linked and linear parts, it is better to present the degree of cross-linking (CL) that occurred as seen in Eq. (3) [40]:

$$CL = \left[1 - \left(\frac{(C/N)_{observed} - (C/N)_{fully\ cross\text{-}linked}}{(C/N)_{fully\ linear} - (C/N)_{fully\ cross\text{-}linked}}\right)\right] \times 100\% \quad (3)$$

where $(C/N)_{observed}$ is the C/N ratio measured by XPS. A fully cross-linked polyamide, $(C/N)_{fully\ cross\text{-}linked}$, has a C/N ratio of 6 and a theoretically fully linear polyamide, $(C/N)_{fully\ linear}$, has a C/N ratio of 7.5 [40].

From the results, the TFC membrane has a 91.65% cross-linking. The TFN membranes have lower CL values since the incorporation of the nanotubes might hinder the kinetics of interfacial polymerization. Among the TFN membranes, TFN-3, which has the highest concentration of aluminosilicate single-walled nanotubes, has the lowest CL value of 63.66%.

3.2.2. Surface morphology and roughness

The surface morphology and surface roughness were analyzed using SEM and AFM to examine the effect of aluminosilicate SWNT incorporation. The SEM images of the top surface and cross-section of TFC and TFN-3 membranes are shown in Fig. 7. Both TFC and TFN-3 membranes have a rugose structure with nodular surface structures common to polyamide films [31]. The TFC membrane (Fig. 7I–A) has a denser structure, with the nodules well-distributed all throughout the plane, compared to the TFN-3 membrane. The TFN-3 membrane (Fig. 7I–B), on the other hand, appears to have lesser nodules but has more visible "leaf-like" outgrowths or "stipules". It seems that the presence of hydroxyl groups on the walls of the aluminosilicate nanotubes provides a barrier for diffusion limited reaction of polymerization. This additional breadth of reaction zone, compared with the case of TFC could produce the "leaf-like" morphology. The leaf-like outgrowths happen throughout the active layer, with certain areas enhanced for higher concentration of TFNs. The existence of these hydrophilic aluminosilicate nanotubes in the organic phase may also augment the miscibility of the aqueous and organic phases during interfacial polymerization, in the same case as zeolites. Lind et al. reported that when zeolites in the hexane phase encounter hydrated MPD from the aqueous phase, the nanostructures will hydrate and release heat, which could locally enhance the miscibility of the aqueous and organic phases [40]. The cross-section images of the TFC and TFN-3 membranes presented in Fig. 7II-A and II-B, also support the explanation of Lind et al. While both polyamide layers have thickness ranging from 100–400 nm, the active layer of the TFN-3 membrane has higher thickness deviation compared to that of the TFC membrane.

Fig. 8 shows the 5 μm × 5 μm three-dimensional AFM images of the thin-film composite membranes, with and without aluminosilicate nanotubes. The root mean square roughness (R_q), root average arithmetic roughness (R_a) and root peak-to-valley distance (R_{pv}) with standard deviation of the membrane surface are listed in Table 2.

From the AFM images, one can observe that TFC and TFN membranes have the characteristic "ridge-and-valley" structure of polyamide distributed throughout the plane [41]. The incorporation of aluminosilicate nanotubes into the TFN polyamide matrix (Fig. 8B–D) somehow creates more variable and bigger ridges. This observation is in conjunction with the SEM images wherein the TFN membranes generated more obvious "leaf-like" folds, which correspond to the ridges seen in AFM. As the concentration of the aluminosilicate nanotubes is increased, R_q, R_a and

R_{pv} values, as listed in Table 2, also increased in the nanoscopic level. The reason is because of the affinity of the MPD aqueous solution towards the hydrophilic nanotubes driving the diamine to diffuse faster towards the IP zone. This evanescent flow towards the nanotubes in the hexane phase increases the diffusion rate of diamines into the organic solution of acid chlorides and increases the diamine concentration in the organic phase causing changes in the distribution of the reaction sites and the amide linkage formation. As a consequence, varying thicknesses with higher peaks and lower valleys are formed.

3.3. Water permeability and permeance

The relationship between the water flux and the transmembrane pressure for the TFC and TFN membranes is illustrated in Fig. 9A. The water permeability of all the membranes increased with increasing applied pressures since the driving force for permeation of water was enhanced. As the aluminosilicate SWNT content in the polyamide layer increases, the water flux also increases. The prepared polyamide TFC shows a water flux value of 10.5 LMH at 16 bar. This value increased to almost 50% as the aluminosilicate nanotubes (TFN-1) were incorporated to polyamide matrix. The pure water flux increased to as high as 24.6 LMH, a 1.5-fold magnitude increase, as 0.59 wt.% of aluminosilicate nanotubes in PA (TFN-3) was incorporated. This water flux surge may be attributed to the water permeation through the interstitial small cavity in the cross-linked site, the interspace between the clusters of networks [42], and increased preferential flow of water molecules through the hydrophilic aluminosilicate nanotubes.

The thickness-normalized pure water permeance values of the TFC and TFN membranes were calculated by taking into account the thickness of the polyamide selective layers. As can be seen from Fig. 9B, the permeance values of the membranes are enhanced with increasing imogolite content in the polyamide active layer. A rise in the permeance value is observed as aluminosilicate SWNT is incorporated within the polyamide matrix. When 0.59 wt.% of aluminosilicate nanotubes in PA (TFN-3) was incorporated, the permeance was enhanced by about 160%, compared to that of TFC membrane. It should be noted that the increase in the pure water permeance of the TFN membranes can be attributed to presence of the hydroxyl groups of the inner walls of the aluminosilicate SWNTs which permits increased preferential water flow.

However, it should be noted that the flux increase is due, not only to the hydrophilic channel of nanotubes, but also to lower crosslinking density. It is well known that water flux increases as the crosslinking density of polyamide layers decreases. In order to understand the effect of provided nano-channels via hydrophilic nanotubes in PA layers, rejection of two salts was evaluated. As can be seen in Fig. 10, the salt (NaCl and Na_2SO_4) rejection of the low pressure RO membranes was measured with different compositions of aluminosilicate SWNT in the polyamide matrix. It can be seen that both NaCl and Na_2SO_4 salt rejections were enhanced. However, increase in NaCl salt rejection is less pronounced, especially when error bars are taken into consideration.

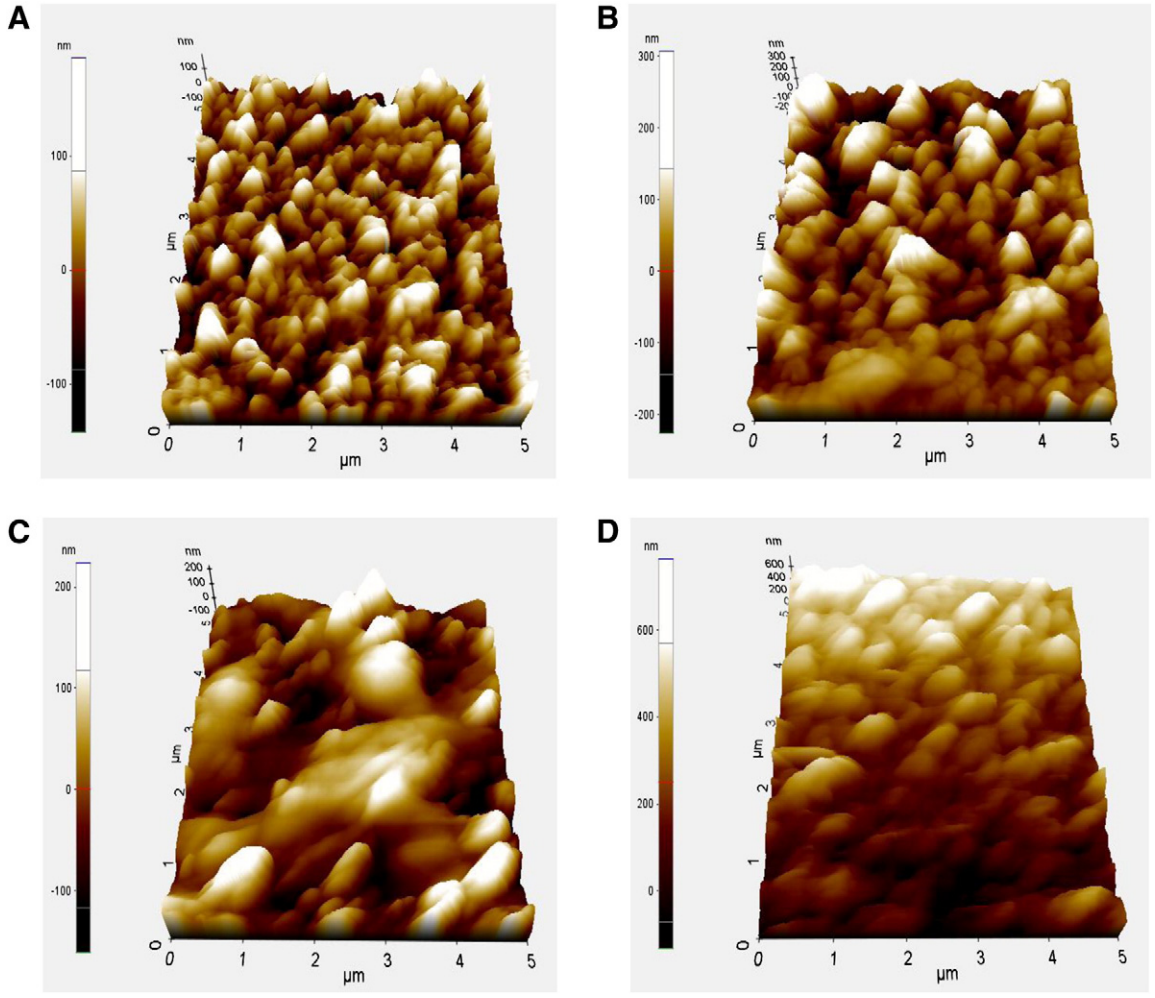

Fig. 8. AFM images of (A) TFC, (B) TFN-1, (C) TFN-2, and (D) TFN-3 membranes.

Table 2
The thickness (L) of the polyamide layers of the membranes determined using SEM, and root mean surface roughness (R_q), root average arithmetic roughness (R_a), and root peak-to-valley (R_{pv}) values of the TFC and TFN membranes on a 5 μm × 5 μm frame.

Sample	L (nm)	R_q (nm)	R_a (nm)	R_{pv} (nm)
TFC	321.33 ± 4.16	24.49 ± 3.82	20.46 ± 4.54	118.78 ± 17.21
TFN-1	361.33 ± 8.33	46.18 ± 1.50	38.08 ± 1.55	194.82 ± 14.12
TFN-2	382.00 ± 4.00	52.55 ± 4.96	42.47 ± 6.36	221.18 ± 3.83
TFN-3	394.67 ± 6.11	64.57 ± 11.26	50.79 ± 8.97	257.52 ± 18.73

Since the TFC and TFN membranes are made by the interfacial polymerization reaction of a monomeric polyamine with a polyfunctional acyl halide, carboxyl and amine functional groups may be expected on the membrane surfaces. This explains a noticeably higher rejection of divalent ions (SO_4^{2-}) compared to that of monovalent ions (Cl^-) because of the higher charge density of SO_4^{2-} ions compared to Cl^- ions. Moreover, the higher rejection of TFC membrane obtained for Na_2SO_4 (R = 96.89%) with respect to NaCl (R = 95.64%) can be ascribed to steric effects [43,44].

The incorporation of aluminosilicate SWNTs in the polyamide layer gives an additional effect on the increase in salt rejection. Since the surface chemistry of the tubular pores of imogolite is negatively charged [45], the nanochannels can use both steric hindrance and electrostatic repulsion to achieve ion rejection [46]. To further

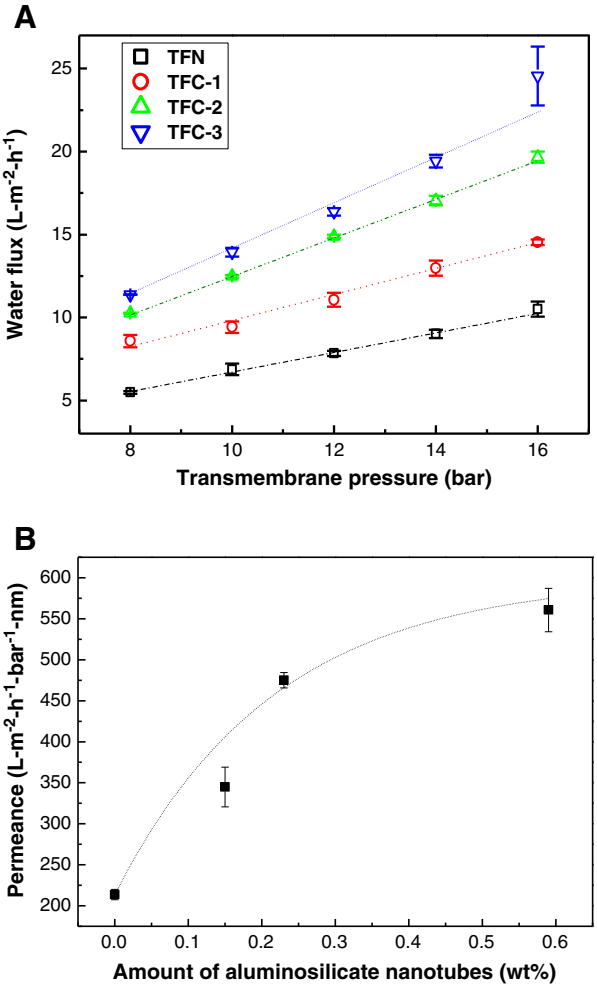

Fig. 9. Water permeability and permeance experiments for TFC and TFN membranes. (A) Relationship of pure water flux with respect to transmembrane pressure for TFC and TFN membranes with increasing aluminosilicate SWNT content. (B) Permeance values of TFC and TFN membranes with increasing aluminosilicate SWNT content.

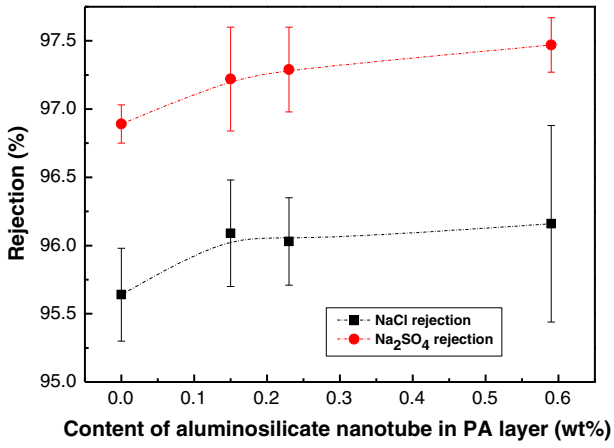

Fig. 10. Salt rejection for the TFC and TFN membranes made with increasing aluminosilicate SWNT concentration.

explain this, bulk diffusivity, hydrated and Stokes radii of the ions, and Debye length listed in Table 3 were considered. Debye length was calculated using Eq. (4) [47]:

$$\lambda_D = \left(\frac{\varepsilon_0 \varepsilon_r k_B T}{2 N_A e^2 I}\right)^{1/2} \quad (4)$$

where ε_0 and ε_r are the vacuum and relative permittivity, respectively, k_B is the Boltzmann constant, T is absolute temperature, e is the elementary charge, N_A is the Avogadro number, and I is the ionic strength of the solution.

The Debye length was calculated to consider the exclusion mechanism that accounts for the effect of the Donnan membrane equilibrium. It is well-known that the Donnan model stipulates a definitive explanation of the electrochemical equipoise formed during interaction of the salt solution and the charged membrane, in this case, the polyamide selective membrane with and without aluminosilicate SWNTs. The Donnan theory relates the rejection coefficient, *R*, of ideal point-charge ions percolating through a charged membrane [48]:

$$R = 1 - \frac{c_i^m}{c_i} = 1 - \left(\frac{|z_i| c_i}{|z_i| c_i^m + c_x^m}\right)^{|z_i/z_j|} \quad (5)$$

where c_i and c_i^m are the concentrations of co-ions in the solution and in the membrane phase respectively, c_x^m is the membrane charge concentration, *z* is the valence, and subscripts *i* and *j* indicate co-ions and counterions, respectively. Eq. (5) expresses the dependence of ion-exclusion on the Debye length, since c_i can be substituted with

Table 3
Debye length (λ_D) and diffusion coefficient (D) of salt solutions, and hydrated radius (r_h), Stokes radius (r_s), and bulk diffusivity (D_i), of ionic species.

Solution	Concentration (M)	λ_D (nm)	D (10^{-9} m^2/s)
NaCl	0.034	1.57[a]	1.61[b]
Na_2SO_4	0.014	1.55[a]	1.23[b]
Ion	**r_s (nm)**	**r_h (nm)**	**D_i (10^{-9} m^2/s)**
Na^+	0.184[c]	0.276[c]	1.334[c]
Cl^-	0.121[d]	0.332[d]	2.032[d]
SO_4^{2-}	0.230[d]	0.379[d]	1.065[d]

[a] Calculated using Eq. (4).
[b] Data acquired from [43].
[c] Data acquired from [46].
[d] Data acquired from [47].

α/λ_D^2, where α is defined as $\frac{\varepsilon_0\varepsilon_r k_B T}{N_A e^2\left(z_i^2+|z_i z_j|\right)}$ [46]. For a charged nanotube with diameter greater than the permeating ion, exclusion of co-ions is expected when the range of ion electrostatic interaction (λ_D) with the pore charges is larger than the pore size [47]. Since for both NaCl and Na_2SO_4, $\lambda_D > d_i$, it is logical to presume that the rejection of the chloride and sulfate salts will be a function of the Donnan potential.

Taking into account the contribution of the negative ions, since both solutions have the same Na^+ cation, rejection of SO_4^{2-} ions will be higher than the Cl^- ions. The reason can be ascribed to sieving effects since r_s and r_h of the divalent anion are larger compared to the monovalent anion. Also, both the solution and the ionic diffusion coefficients of NaCl and Cl^- are superior to that of Na_2SO_4 and SO_4^{2-} which could explain the faster diffusion of the former through the polymer matrix and nanotubes. The difference in diffusion coefficients ($D_{Cl^-} = 2.032 \times 10^{-9}$ m^2/s > $D_{SO_4^{2-}} = 1.065 \times 10^{-9}$ m^2/s; $D_{NaCl} = 1.61 \times 10^{-9}$ m^2/s > $D_{Na_2SO_4} = 1.23 \times 10^{-9}$ m^2/s) between the two salts, as listed in Table 3, determines the higher TFN membrane retentions (for TFN-3, $R_{Na_2SO_4} = 97.47\% > R_{NaCl} = 96.16\%$).

4. Conclusions

Thin film nanocomposite low pressure RO membranes were successfully prepared through interfacial polymerization of polyamide on a polysulfone support. Aluminosilicate single-walled nanotubes were synthesized and were incorporated to the polyamide matrix using a single pass flow method. The synthesized nanotubes were comparable to the natural and synthesized imogolite having $d_i =$ 1.01–1.17 nm and $d_o = 2.7$–3.1 nm, as observed in the TEM, XRD and nitrogen adsorption measurements. The chemical structure, morphology, and surface roughness of the membranes were characterized. Results show that the active layer of the membrane consists of carboxyl and amino groups common to aromatic polyamide. The aluminosilicate SWNTs were successfully incorporated within the TFN membranes as seen in the presence of O–Al–O and Al–OH peaks, and increasing values of the elemental Al and Si, in the IR and XPS experiments, respectively. The TFC and TFN membranes exhibited rugose structure with stipules common to polyamide films. AFM images show that TFC and TFN membranes have the characteristic "ridge-and-valley" structure of polyamide distributed throughout the plane. High permeate flux was attained with the preferential water flow through the hydrophilic nanochannels. Higher rejection of divalent ions compared to monovalent ones can be ascribed to Donnan potential and steric effects. The hand-cast thin film nanocomposite membranes exhibit increased permeability and improved rejection which will be helpful for low pressure RO. Once optimized via modern commercial fabricating techniques, the thin film nanocomposite with aluminosilicate SWNTs can be used for higher pressure desalination processes and pose new degrees of freedom not achievable with TFC membranes alone.

Acknowledgments

This research was supported by the Basic Science Research Program through the National Research Foundation (NRF) of Korea funded by the Ministry of Education, Science and Technology (2012R1A1A2006821). This work was also supported by the Korea CCS R&D Center (KCRC) grant funded by the Ministry of Education, Science and Technology (2011-0032169).

References

[1] P.W. Morgan, S.L. Kwolek, Interfacial polycondensation. II. Fundamentals of polymer formation at liquid interfaces, J. Polym. Sci. 40 (1959) 299–327.
[2] J.E. Cadotte, R.J. Petersen, R.E. Larson, E.E. Erickson, A new thin-film composite seawater reverse osmosis membrane, Desalination 32 (1980) 25–31.
[3] Y.H. La, R. Sooriyakumaran, D.C. Miller, M. Fujiwara, Y. Terui, K. Yamanaka, B.D. McCloskey, B.D. Freeman, R.D. Allen, Novel thin film composite membrane containing ionizable hydrophobes: pH dependent reverseosmosis behavior and improved chlorine resistance, J. Mater. Chem. 20 (2010) 4615–4620.
[4] S. Yu, Q. Zhou, S. Shuai, G. Yao, M. Ma, C. Gao, Thin-film composite nanofiltration membranes with improved acid stability prepared from naphthalene-1,3,6-trisulfonylchloride (NTSC) and trimesoyl chloride (TMC), Desalination 315 (2013) 164–172.
[5] G. Kang, M. Liu, B. Lin, Y. Cao, Q. Yuan, A novel method of surface modification on thin-film composite reverse osmosis membrane by grafting poly(ethylene glycol), Polymer 48 (2007) 1165–1170.
[6] B.J. Abu Tarboush, D. Rana, T. Matsuura, H.A. Arafat, R.M. Narbaitz, Preparation of thin-film-composite polyamide membranes for desalination using novel hydrophilic surface modifying macromolecules, J. Membr. Sci. 325 (2008) 166–175.
[7] T. Shintani, H. Matsuyama, N. Kurata, Effect of heat treatment on performance of chlorine-resistant polyamide reverse osmosis membranes, Desalination 247 (2009) 370–377.
[8] A.K. Ghosh, B.-H. Jeong, X. Huang, E.M.V. Hoek, Impacts of reaction and curing conditions on polyamide composite reverse osmosis membrane properties, J. Membr. Sci. 311 (2008) 34–45.
[9] D. Li, H. Wang, Recent developments in reverse osmosis desalination membranes, J. Mater. Chem. 20 (2010) 4551–4566.
[10] V. Baglio, A.S. Arico, A. Di Blasi, P.L. Antonucci, F. Nannetti, V. Tricoli, V. Antonucci, Zeolite-based composite membranes for high temperature direct methanol fuel cells, J. Appl. Electrochem. 35 (2005) 207–212.
[11] S.A. Hashemifard, A.F. Ismail, T. Matsuura, Mixed matrix membrane incorporated with large pore size halloysite nanotubes (HNTs) as filler for gas separation: morphological diagram, Chem. Eng. J. 172 (2011) 581–590.
[12] G. Liu, F. Xiangli, W. Wei, S. Liu, W. Jin, Improved performance of PDMS/ceramic composite pervaporation membranes by ZSM-5 homogeneously dispersed in PDMS via a surface graft/coating approach, Chem. Eng. J. 174 (2011) 495–503.
[13] D.S. Sholl, J.K. Johnson, Making high-flux membranes with carbon nanotubes, Science 312 (2006) 1003–1004.
[14] M.L. Lind, D.E. Suk, T.V. Nguyen, E.M.V. Hoek, Tailoring the structure of thin film nanocomposite membranes to achieve seawater RO membrane performance, Environ. Sci. Technol. 44 (2010) 8230–8235.
[15] M. Fathizadeh, A. Aroujalian, A. Raisi, Effect of added NaX nano-zeolite into polyamide as a top thin layer of membrane on water flux and salt rejection in a reverse osmosis process, J. Membr. Sci. 375 (2011) 88–95.
[16] P.S. Singh, V.K. Aswal, Characterization of physical structure of silica nanoparticles encapsulated in polymeric structure of polyamide films, J. Colloid Interface Sci. 326 (2008) 176–185.
[17] S.Y. Lee, H.J. Kim, R. Patel, S.J. Im, J.H. Kim, B.R. Min, Silver nanoparticles immobilized on thin film composite polyamide membrane: characterization, nanofiltration, antifouling properties, Polym. Adv. Technol. 18 (2007) 562–568.
[18] E.-S. Kim, G. Hwang, M.G. El-Din, Y. Liu, Development of nanosilver and multi-walled carbon nanotubes thin-film nanocomposite membrane for enhanced water treatment, J. Membr. Sci. 394–395 (2012) 37–48.
[19] B.-H. Jeong, E.M.V. Hoek, Y. Yan, A. Subramani, X. Huang, G. Hurwitz, A.K. Ghosh, A. Jawor, Interfacial polymerization of thin film nanocomposites: a new concept for reverse osmosis membranes, J. Membr. Sci. 294 (2007) 1–7.
[20] D.S. Sholl, J.K. Johnson, Materials Science: making high-flux membranes with carbon nanotubes, Science 312 (2006) 1003–1004.
[21] M. Majumder, N. Chopra, R. Andrews, B.J. Hinds, Nanoscale hydrodynamics: enhanced flow in carbon nanotubes, Nature 438 (2005) 44–45.
[22] V.C. Farmer, M.J. Adams, A.R. Fraser, F. Palmieri, Synthetic imogolite: properties, synthesis, and possible application, Clay Miner. 18 (1983) 459–472.
[23] P.D.G. Cradwick, V.C. Farmer, J.D. Russell, C.R. Masson, K. Wada, N. Yoshinaga, Imogolite, a hydrated aluminium silicate of tubular structure, Nature 240 (1972) 187–189.
[24] F. Ohashi, S. Tomura, K. Akaku, S. Hayashi, S.-I. Wada, Characterization of synthetic imogolite nanotubes as gas storage, J. Mater. Sci. 39 (2004) 1799–1801.
[25] E. Belorizky, P.H. Fries, A. Guillermo, O. Poncelet, Almost ideal 1D water diffusion in imogolite nanotubes evidenced by NMR relaxometry, Chem. Phys. Chem. 11 (2010) 2011–2026.
[26] B. Creton, D. Bougeard, K.S. Smirnov, J. Guilment, O. Poncelet, Molecular dynamics study of hydrated imogolite. 2. Structure and dynamics of confined water, Phys. Chem. Chem. Phys. 10 (2008) 4879–4888.
[27] K. Yamamoto, H. Otsuka, S.I. Wada, D. Sohn, A. Takahara, Preparation and properties of [poly(methyl methacrylate)/imogolite] hybrid via surface modification using phosphoric acid ester, Polymer 46 (2005) 12386–12392.
[28] H. Yang, Y. Chen, Z. Su, Microtubes via assembly of imogolite with polyelectrolyte, Chem. Mater. 19 (2007) 3087–3089.
[29] D.Y. Kang, H.M. Tong, J. Zang, R.P. Choudhury, D.S. Sholl, H.W. Beckham, C.W. Jones, S. Nair, Single-walled aluminosilicate nanotube/poly(vinyl alcohol) nanocomposite membranes, ACS Appl. Mater. Interfaces 4 (2012) 965–976.
[30] K. Yamamoto, H. Otsuka, S.-I. Wada, D. Sohn, A. Takahara, Transparent polymer nanohybrid prepared by in situ synthesis of aluminosilicate nanofibers in poly(vinyl alcohol) solution, Soft Matter 1 (2005) 372–377.
[31] A.K. Ghosh, E.M.V. Hoek, Impacts of support membrane structure and chemistry on polyamide–polysulfone interfacial composite membranes, J. Membr. Sci. 336 (2009) 140–148.
[32] G.N.B. Baroña, B.J. Cha, B. Jung, Negatively charged poly(vinylidene fluoride) microfiltration membranes by sulfonation, J. Membr. Sci. 290 (2007) 46–54.

[33] K. Wada, N. Yoshinaga, H. Yotsumoto, K. Ibe, S. Aida, High resolution electron micrographs of imogolite, Clay Miner. 8 (1970) 487–489.
[34] W.C. Ackerman, D.M. Smith, J.C. Huling, Y.W. Kim, J.K. Bailey, C.J. Brinker, Gas/vapor adsorption in imogolite: a microporous tubular aluminosilicate, Langmuir 9 (1993) 1051–1057.
[35] L.M. Liz-Marzan, A.P. Philipse, Stable hydrosol of metallic and bimetallic nanoparticles immobilized on imogolite fibers, J. Phys. Chem. 99 (1995) 15120–15128.
[36] G. Horvath, K. Kawazoe, Method for the calculation of effective pore size distribution in molecular sieve carbon, J. Chem. Eng. Jpn. 16 (1983) 470–475.
[37] S. Konduri, S. Mukherjee, S. Nair, Controlling nanotube dimensions: correlation between composition, diameter, and internal energy of single-walled mixed oxide nanotubes, ACS Nano 1 (2007) 393–402.
[38] S. Mukherjee, V.M. Bartlow, S. Nair, Phenomenology of the growth of single-walled aluminosilicate and aluminogermanate nanotubes of precise dimensions, Chem. Mater. 17 (2005) 4900–4909.
[39] Y. Jin, W. Wang, Z. Su, Spectroscopic study on water diffusion in aromatic polyamide thin film, J. Membr. Sci. 379 (2011) 121–130.
[40] M.L. Lind, A.K. Ghosh, A. Jawor, X. Huang, W. Hou, Y. Yang, E.M.V. Hoek, Influence of zeolite crystal size on zeolite–polyamide thin film nanocomposite membranes, Langmuir 25 (2009) 10139–10145.
[41] N.K. Saha, S.V. Joshi, Performance evaluation of thin film composite polyamide nanofiltration membrane with variation in monomer type, J. Membr. Sci. 342 (2009) 60–69.
[42] S.H. Kim, S.-Y. Kwak, T. Suzuki, Positron annihilation spectroscopic evidence to demonstrate the flux-enhancement mechanism in morphology-controlled thin-film-composite (TFC) membrane, Environ. Sci. Technol. 39 (2005) 1764–1770.
[43] J.M.M. Peeters, J.P. Boom, M.H.V. Mulder, H. Strathmann, Retention measurements of nanofiltration membranes with electrolyte solutions, J. Membr. Sci. 145 (1998) 199–209.
[44] J. Schaep, C. Vandecasteele, A.W. Mohammad, W.R. Bowen, Modelling the retention of ionic components for different nanofiltration membranes, Sep. Purif. Technol. 22–23 (2001) 169–179.
[45] J.P. Gustafsson, The surface chemistry of imogolite, Clays Clay Miner. 49 (2001) 73–80.
[46] F. Fornasiero, H.G. Park, J.K. Holt, M. Stadermann, C.P. Grigoropoulos, A. Nov, O. Bakajin, Ion exclusion by sub-2-nm carbon nanotube pores, Proc. Natl. Acad. Sci. U. S. A. 105 (2008) 17250–17255.
[47] B. Tansel, Significance of thermodynamic and physical characteristics on permeation of ions during membrane separation: hydrated radius, hydration free energy and viscous effects, Sep. Purif. Technol. 86 (2012) 119–125.
[48] J. Schaep, B. Van der Bruggen, C. Vandecasteele, D. Wilms, Influence of ion size and charge in nanofiltration, Sep. Purif. Technol. 14 (1998) 155–162.